Graphene-based resistive humidity sensor for in-situ monitoring of drying shrinkage and intrinsic permeability in concrete

Bérengère Lebental, Waleed Moujahid, Chang-Soek Lee, Jean Luc Maurice, Costel-Sorin Cojocaru

Graphene-based resistive humidity sensor for *in-situ* monitoring of drying shrinkage and intrinsic permeability in concrete

B. Lebental[1,2], W. Moujahid[1,2], C.-S. Lee[2], J.-L. Maurice[2] and C.S. Cojocaru[2]

[1]*Université Paris-Est, IFSTTAR, Paris, France*
berengere.lebental@ifsttar.fr, waleed.moujahid@ifsttar.fr
[2]*Laboratoire de Physique des Interfaces et Couches Minces (LPICM), UMR 7647, Ecole Polytechnique-CNRS, Palaiseau, France*
changseok.lee@polytechnique.edu, jean-luc.maurice@polytechnique.edu, costel-sorin.cojocaru@polytechnique.edu

ABSTRACT

Nanosensors dedicated to the structural health monitoring of concrete structures have been only marginally studied. They would however be particularly well-suited to monitor durability-related processes, as these phenomena involve transport of gas and liquids through micro and nano-porosity. In this paper we discuss the relevance and feasibility of embedding relative humidity nanosensors within concrete. It appears that the localized, continuous knowledge of relative humidity within a concrete structure could provide a useful insight into drying shrinkage; it could also contribute to improved intrinsic permeability measurements, leading to improved assessment of structural durability. For the task, we propose a low-cost, downscalable resistive device made of a 10 nm graphene sheet grown directly on glass and atop which are ink-jet printed silver electrodes. The device resistance increases significantly with relative humidity (RH), especially above 40% RH. Relative amplitude of variations are only of about 3% for the two tested devices, but absolute variations (80 Ω and 480 Ω) appear measurable by a low-cost and robust signal conditioning electronics. Thus, the idea of using our graphene-based resistive device for embedded humidity monitoring in concrete appears quite promising.

Keywords:structural health monitoring, relative humidity, durability, graphene, nanosensors.

1. Nanosensors for structural health monitoring (SHM) of concrete structures

Nanomaterials are highly sensitive to environmental changes because of their high surface-over-volume ratio. To exploit this property, there has been a large variety of nanosensors[1] development. Nanoelectromechanical systems (NEMS) such as suspended cantilevers [1-2] or electronic devices such as carbon nanotubes field effect transistors [3-4] are used as sensors in various applications ranging from lab-on-chips [5] and artificial noses [6] to aerospace technologies [7], for instance to measure pressure [8] or to detect specific chemical or biological agents [9].

These new sensors concept have not really inspired the field of concrete SHM yet. One of the main obstacles seems to lie in the difficulty to identify relevant monitoring targets compatible with size and sensitivity of nanosensors. Indeed, nanosensors appear as small, fragile and "clean" objects whereas civil engineering structures are seen as large, disordered and "dirty" structures.

However, it is now well-known that macroscopic properties of cementitious materials depend on nanoscale features [10-11]. Durability especially is determined by transport of noxious gas or ions through the micro- and nanoporosity [12]. Thanks to extended *ex-situ* studies, the mi-

[1] We call nanosensor a sensing device with at least one characteristic size smaller than 100 nm. For instance, we might call nanosensor a device with a 10 nm thin, 10 µm x 10 µm active surface.

cro and nanoscale properties of the porosity have been translated into macroscopic durability indicators such as porosity, permeability, diffusivity, which are easier to account for in building codes and international norms [13].

But to this day, no *in-situ* measurement method exists for these durability indicators, mostly because of their tight relationship with nanoscale properties. Indeed, most concrete SHM techniques are based on the use of propagating waves with wavelength larger than one millimeter [14], thus automatically homogenizing the porosity.

In 2008, we put forward nanosensors as ideal candidates for *in-situ* monitoring of durability indicators, as their nanoscale features would enable to account for nanoscale heterogeneity of concrete [15]. Since then, we have worked on prototyping of appropriate nanosensors as well as on clarifying the quantities they would be sensitive too.

Our first device concept consisted in an ultrasonic microtransducer based on a 10 nm thin carbon nanotubes vibrating membrane emitting high frequency (100 MHz-1GHz) ultrasonic waves and detecting them with a micrometric lateral resolution [16]. We showed experimentally element of the feasibility of such a device [17]. Numerical experiments indicated that the device would be relevant to monitor micropores size and content [18], which would in turn prove invaluable for durability assessment. However, the complexity of the sensing principle and electronics will require long-term development and optimization before its relevance as an embeddable sensor can be demonstrated experimentally.

So we propose here another sensor concept, a down-scalable, low-cost graphene-based resistive device for embedded relative humidity monitoring within concrete. In the rest of this paper, we discuss the applicative relevance of embedding relative humidity sensors in concrete and we present our sensing device and its performances.

3. Possible applications of embedded relative humidity monitoring in concrete

Let us assume in this section that embedded relative humidity sensors were operational within concrete. They would provide over time localized measurement of the inner relative humidity of the studied material.

3.1. In-situ, localized estimation of capillary pressure and liquid water saturation

The first use of such data could be the determination of the **capillary pressure** at the local scale. Indeed, once gaseous equilibrium is achieved within the open porosity, Kelvin's law links the capillary pressure p_c to the relative humidity h_r by the relationship

$$p_c = -\frac{\rho_l RT}{M_l} \ln h_r \tag{1}$$

where ρ_l and M_l are respectively the liquid water density and molar mass, R the constant of ideal gas and T the temperature [19].

Provided sorption isotherms are known for the studied material [20], once the capillary pressure is determined in the vicinity of each sensor, one can use these isotherms to derive the local value for the **liquid water saturation** S_l, defined as the ratio of the porosity ϕ_l occupied by liquid water to the total porosity ϕ:

$$S_l = \frac{\phi_l}{\phi} \quad \text{and} \quad S_l \approx \left(1 + \left(\frac{p_c}{\mathrm{M}} \right)^{\frac{1}{1-m}} \right)^{-m} \tag{2}$$

with M ≈ 10-100 MPa and m ≈ 0.45-0.55 two constants depending on the material [19-21]. Figure 1a displays capillary pressure and liquid water saturation with respect to relative humidity.

Usually, liquid water saturation is determined by weighing the sample, so it can only be determined *ex-situ* and at a macroscopic scale. Here we open up the path toward determining *in-situ* and locally liquid water saturation. Such information could for instance be used directly on the construction site to ascertain that the hydration process follows expectations. If not, corrective measures could thus be undertaken very early after casting, thus reducing the risk (and the associated costs) for non-complying concrete.

3.2. In-situ estimation of the drying shrinkage

Drying shrinkage is responsible for significant degradations of concrete materials, especially in high performance materials [22]. It was shown by a poromechanics approach based on the equivalent pore pressure concept [19] that drying shrinkage depends strongly on both capillary pressure and liquid water saturation.

Denoting ε the **drying shrinkage**, we have the relationship

$$d\varepsilon = \frac{bS_l}{K} dp_c = -\frac{b\rho_l RT}{KM_l} S_l \frac{dh_r}{h_r} \tag{3}$$

with b Biot's coefficient and K the bulk modulus of the drained material. This relationship is valid at the local scale. Assuming we know the relative humidity repartition $h_r(x,t)$ from embedded sensors, we can deduce from (3) the shrinkage by unit length $d\varepsilon / dx(x,t)$ from which an integration step can yield the total shrinkage. The density of humidity sensors will control the accuracy of the result.

Using the differential expression (3) to determine shrinkage instead of the global expression involving external relative humidity and sorption isotherms [19] presents a significant advantage because for most concretes, especially high performance ones, it may take years for the inner relative humidity to match the external relative humidity. As a consequence, shrinkage remains for years considerably different from its predicted value. As an illustration, in figure 1b, we have plotted with respect to time the difference between the shrinkage values calculated by the differential expression (3) and the global shrinkage value deduced from the external humidity.

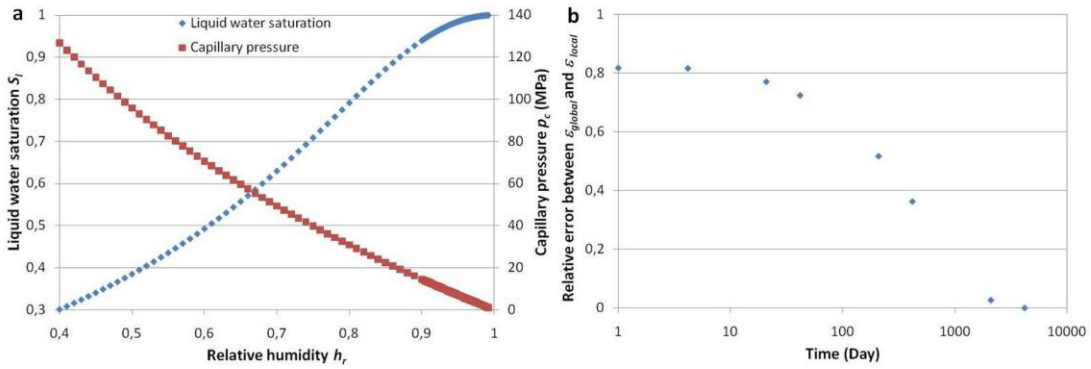

Fig. 1. a) Capillary pressure and liquid water saturation with respect to relative humidity, at 300°K, for *m=0.5*, M=*40MPa*. b) Relative error between the shrinkage value resulting from local ε_{local} and global ε_{global} calculations using simulated data for the relative humidity $h_r(x,t)$, which is assumed to verify the heat equation with diffusity $7x10^{-6}$ *m²/hour* in a beam with length *1 m;* external humidity is set at *0.5; m=0.5*, M=*40MPa, K=13 GPa, T=300°K.*

By processing the data from localized humidity sensors using the differential expression (3) for shrinkage, we would obtain a continuous measurement of shrinkage and consequently an improved prediction of shrinkage related cracking. We could for instance detect the onset of shrinkage, hence facilitating the implementation of mitigation strategies.

3.3. In-situ estimation of the intrinsic permeability

Gas and liquid permeability coefficients play a key role in the durability of concrete structures, insofar as they control transport through the material of gas and liquid, water especially.

In particular, permeability regulates drying, so that one of the methods to determine intrinsic permeability is based on inverse analysis of the isothermal drying equations [21]: these equations are solved numerically for various values of the intrinsic permeability so as to yield relative humidity and liquid water saturation with respect to position and time in the studied material. The outputs are used to fit experimental plots of relative weight loss (which depends on liquid water saturation) versus time; the best fit yields the value of the intrinsic permeability of the sample.

In such framework, the localized, continuous outputs of relative humidity sensors could be directly used to calibrate the drying model by inverse analysis and then determine the **intrinsic permeability**. One would expect a significant gain in accuracy from using localized data instead of the global, indirect, relative weight loss parameter. Evaluation duration could probably be shortened, as there would be much more data to fit precisely the models.

In a further step, this model-based method could even be used *in-situ*, informing continuously the user on the permeability of the structure. Increase of permeability, associated to crack opening and durability loss, could thus be detected early and the structure repaired.

4. Low-cost, down-scalable graphene based humidity sensor for concrete

4.1. Device concept

The ability to measure continuously relative humidity within concrete would thus open up new paths for concrete *in-situ* monitoring. The sensors required for the task cannot be expensive, as they will be abandoned within the material. They also need to be robust, as concrete is a harsh material. They would be preferably small, in order to minimize perturbation of the medium. Smaller devices could also be embedded in larger number.

We present here a nanodevice that appears to meet all these requirements and would thus be an outstanding candidate for embedding. The device is composed of a glass substrate covered by few-layer-graphene with silver electrodes on top (Figure 1). We have studied how the resistance between two neighboring electrodes depends on relative humidity.

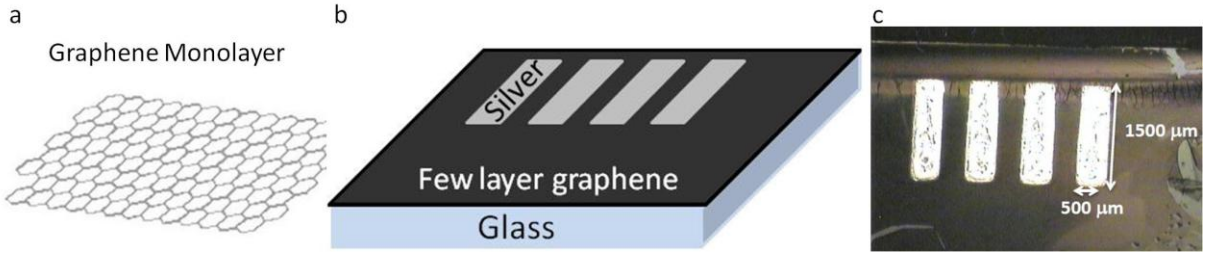

Fig. 2 a) A graphene layer is an atomically thin (0.3 nm) layer of carbon atoms arranged into a honeycomb lattice. b) Scheme and c) image of the device: a glass substrate is covered by few-layer-graphene. Silver electrodes are deposited on the graphene to form contacts.

4.2. Low-cost fabrication process

Early preparation routes of graphene consisted in the mechanical or chemical exfoliation of graphite [23] or in the epitaxial growth on SiC by high temperature annealing [24]. Newer, often more reproducible methods involve crystallization of carbon atoms on metallic catalytic substrates [25]. However, the conducting substrates prevent subsequent electrical measurements. The high temperature requirement (>900°C) prevents growth on low-cost substrates such as glass and plastics. Most often graphene sheets need to be transferred after growth onto other substrates, which is a defect inducing, time consuming process [26].

The alternative CH_4/H_2 PECVD (Plasma Enhanced Chemical Vapor Deposition) process we developed [27-28] enables graphene growth on a glass substrate heated at 450°C only. A continuous sheet (several cm²) of few layer graphene grows directly at the interface between a 200 nm catalytic Nickel layer and the glass substrate.

We fabricated two samples by this technique. Based on optical absorption data, sheets are averagely less than 10 nm thick. Thickness is not constant along the sheets. Raman and TEM observation indicate that the graphene is imperfectly crystallized [29].

As the graphene sheets are grown directly on an insulating substrate, they do not need to be transferred before measuring the sheet resistance. One only needs to deposit contacts; this can be done by various clean room methods, such as metal evaporation combined with optical lithography. However, clean room processes are expensive and often complicated.

We opted for a low-cost and down-scalable process, the ink-jet printing of silver electrodes using INKTEC TEC-IJ-010 silver ink in a Dimatix DMP-2800 materials printer. Current printing resolution is about 50 µm and is expected to reach 1 to 5 µm with the newest Dimatix's printer, so electrodes as small as 10 µm² could be fabricated.

We printed on the two samples series of four 500 µm x 1000 µm parallel rectangular patterns separated by 500 µm. After 130° heating for 5 minutes, we obtained the desired electrodes.

This last step concluded the fabrication process, which is summarized Figure 3. Key aspects are the **low-temperature growth of graphene on a low-cost substrate followed by the low-cost printing of electrodes.**

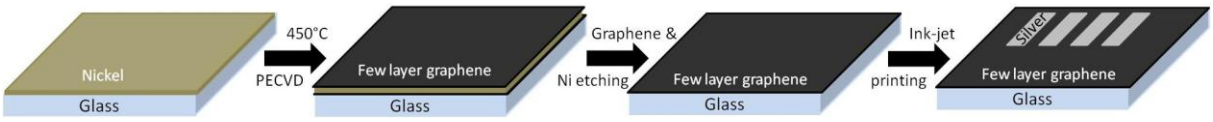

Fig. 3 Device fabrication process. When achieving CH_4/H_2 PECVD on a 450°C heated glass substrate with a Ni top layer, graphene sheets grow on both side of the Ni layer. A step of graphene etching followed by a step of Ni etching leave only the interfacial graphene on top of the glass substrate. Afterward, silver electrodes are ink-jet printed on top of the graphene sheet.

4.3. Sensitivity to humidity

The resistive behavior of the two devices was studied by the following method: two neighboring electrodes are contacted by microtips and the I-V characteristic is acquired using a MATLAB controlled Keithley 2612 Source Meter. The I-V characteristic is linear which indicates the ohmic behavior of the device. We deduce the resistance by least-square fitting this

curve. At about 45 % relative humidity (RH), resistances were found to be 15.0 kΩ and 2.2 kΩ for the two devices. The discrepancy may be explained by the inhomogeneous thickness of both graphene sheets.

We then characterized both devices under increasing relative humidity by the following process: the devices are placed in our home-made climatic characterization chamber heated at 25°C; RH is first decreased down to 5 % by pouring N_2 into the chamber, then it is increased by 5% to 10 % steps; meanwhile resistance between electrodes is measured approximately every 4 seconds; each step is maintained until stabilization of RH in the chamber and stabilization of the device resistance.

Figure 4a shows relative humidity and resistance versus time for the device with 2.2 kΩ resistance. Stabilization time can reach up to 1 hour at 25°C, especially for high RH values. To determine the sensitivity of the device, relative humidity and resistance are averaged over the final part of each step, where both quantities are stabilized. Figure 4b shows the resulting Resistance versus RH plot. Error bars are determined using the infinite norm errors $\max_{step}(RH - < RH >)$ and $\max_{step}(R - < R >)$. They are in the 0.1% range.

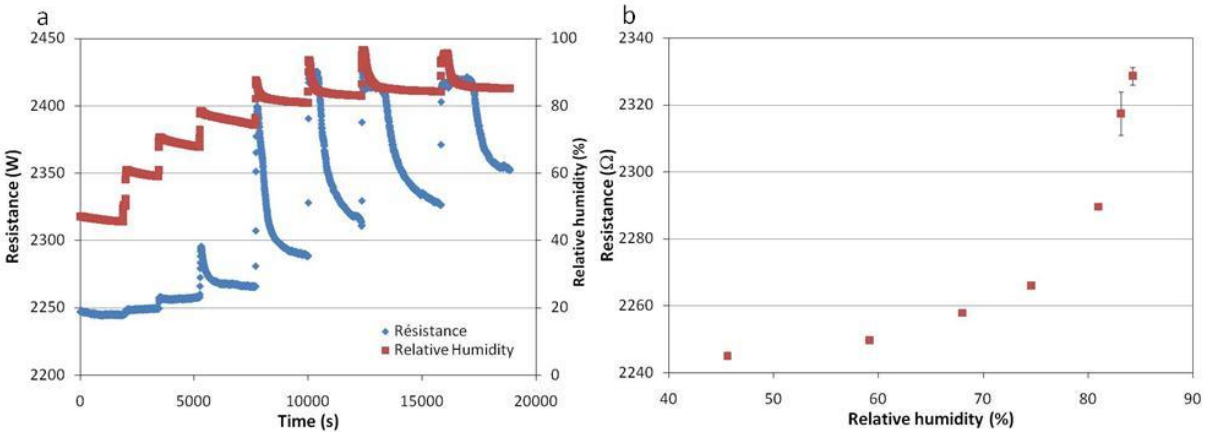

Fig. 4 a) Relative humidity and resistance versus time and b) Resistance versus relative humidity for the device with 2.2 kΩ resistance.

For both devices, the **sensitivity to humidity is clear, especially above 40% RH**. For the 2.2 kΩ device, the resistance increases by 80 Ω (4%) between 45 % and 85 %; for the 15.0 kΩ, by 480 Ω (3%) between 5 % and 65 %.

3.4 *Toward signal conditioning and integration for embedded sensing*

Although relative resistance variations are small, absolute resistance variations appear large enough to be measured by discrete electronic components. For instance the variable resistance could be put in series with a temperature and humidity calibrated resistance and measured via a voltage divider; an operational amplifier in follow-up configuration could then isolate this conditioning circuit from the rest of the system, for example from the numerisation electronics. Let us underline here that the required signal conditioning is expected to be much simpler to implement, less expensive and much more robust than the conditioning required for most low-cost humidity sensors, as those are based on a variable capacitance.

Once the signal is conditioned, the obtained nanosensors may be used individually or within sensors arrays. They will then need to be integrated into larger embeddable autonomous micro-systems that will provide them with energy, communicate the gathered information to the user and have basic computational capabilities. Features and examples of such embedded mi-

cro-systems are discussed for instance in [30-31]. Special care will also be required in the packaging of the micro-systems, in order for them to survive the harsh environmental conditions in concrete [32].

5. Conclusions

The relevance of embedding relative humidity nanosensors in concrete is discussed. Among others, they could monitor drying shrinkage and provide an *in-situ* measurement method for intrinsic permeability. As sensor candidate, we prototyped a low-cost, downscalable resistive device consisting in 10 nm graphene sheet grown directly on glass and contacted by ink-jet printed silver electrodes. The two characterized devices are especially sensitive to relative humidity above 40%. Considering the amplitude of resistance variations, a robust and low-cost signal conditioning electronics appears compatible with the devices.

Acknowledgments

BL would like to thank Véronique Baroghel Bouny (IFSTTAR), Yvan Bonnassieux (LPICM) and Jean-Charles Vanel (LPICM) for helpful discussions.

References

1. Li M, Tang HX and Roukes ML. Ultra-sensitive NEMS-based cantilevers for sensing, scanned probe and very high-frequency applications. Nature Nanotechnology 2, 114 - 120 (2007)
2. Waggoner PS and Craighead HG. Micro- and nanomechanical sensors for environmental, chemical, and biological detection. Lab Chip, 7, 1238-1255 (2007)
3. Zhang J, Boyd A, Tselev A, Paranjape M and Barbara P. Mechanism of NO2 detection in carbon nanotube field effect transistor chemical sensors. Appl. Phys. Lett. 88, 123112 (2006)
4. Besteman K, Lee JO, Wiertz FGM, Heering HA and Dekker C. Enzyme-Coated Carbon Nanotubes as Single-Molecule Biosensors. Nano Letters 3 (6), 727–730 (2003)
5. Lee M, Baik KY, Noah M, Kwon YK, Lee JO and Hong S. Nanowire and nanotube transistors for lab-on-a-chip applications. Lab Chip 9, 2267-2280 (2009)
6. Chen PC, Ishikawa FN, Chang HK, Ryu K and Zhou C. A nanoelectronic nose: a hybrid nanowire/carbon nanotube sensor array with integrated micromachined hotplates for sensitive gas discrimination. Nanotechnology 20 125503 (2009)
7. Yatsenko VA. The development of nanosensors for space applications. 4th International Conference on Advanced Optoelectronics and Lasers, 210-212 (2008)
8. Xu X, Bercu B, Lime F, Montès L. An innovative NEMS pressure sensor approach based on heterostructure nanowire. Microelectronic Engineering 87, 406–411 (2010)
9. Cui Y, Wei Q, Park H, Lieber CM. Nanowire Nanosensors for Highly Sensitive and Selective Detection of Biological and Chemical Species. Science 293 (5533), 1289-1292 (2001)
10. Bentz DP, Quenard DA, Baroghel-Bouny V, Garboczi EJ, Jennings HM. Modelling drying shrinkage of cement paste and mortar. Part 1. Structural models from nanometres to millimetres. Materials and Structures 28, 450-458 (1995)
11. Scrivener KL, Kirkpatrick RJ. Innovation in use and research on cementitious material. Cement and Concrete Research 38, 128–136 (2008)
12. Baroghel-Bouny V. Water vapour sorption experiments on hardened cementitious materials. Part II: Essential tool for assessment of transport properties and for durability prediction. Cement and Concrete Research 37(3), 438-454 (2007)

13. Baroghel-Bouny V. Which toolkit for durability evaluation as regards chloride ingress into concrete? Part II: Development of a performance approach based on durability indicators and monitoring parameters. Third International RILEM Workshop on Testing and Modelling Chloride Ingress into Concrete, 137 – 163 (2004)
14. Breysse D, Abraham O and Berthier J. Méthodologie d'évaluation non destructive de l'état d'altération des ouvrages en béton. Presse des Ponts et Chaussées (2004)
15. Lebental B, Ghis A and Delevoye E. Procédé et dispositif d'analyse acoustique de microporosites dans un matériau tel que le béton à l'aide d'une pluralité de transducteurs CMUTs incorporés dans le matériau. Patent EN 08 57927 ; WO 2010 057,990 (2008)
16. Lebental B, Ghis A, Delevoye E, Caussiganc JM and Bourquin F. Capacitive ultrasonic micro-transducer made of carbon nanotubes: prospects for the in-situ embedded non destructive testing of durability in cementitious materials. EJECE 15, 649-662 (2011)
17. Lebental B, Ghis A et al. Aligned carbon nanotube based ultrasonic microtransducers for durability monitoring in civil engineering. Nanotechnology 22 395501 (2011)
18. Lebental B, Bourquin F. Elasto-acoustic modelling of a vibrating plate interacting with water confined in a domain of micrometric size. J. Sound and Vibration, to appear, 2012.
19. Coussy O, Dangla P, Lassabatère T and Baroghel-Bouny V. The equivalent pore pressure and the swelling and shrinkage of cement-based materials. Materials and Structures 37(1), 15-20 (2004)
20. Baroghel-Bouny V. Water vapour sorption experiments on hardened cementitious materials; Part I and II. Cement and Concrete Research 37, 414-454 (2007)
21. Baroghel-Bouny V, Mainguy M, Lassabatere T and Coussy O. Characterization and identification of equilibrium and transfer moisture properties for ordinary and high performance cementitious materials. Cement and Conrete Research 29, 1225-1238 (1999)
22. Aïtcin PC. The durability characteristics of high performance concrete: a review. Cement and Concrete Composites 25 (4-5), 409-420 (2003)
23. Novoselov KS, Geim AK et al. . Two-dimensional gas of massless Dirac fermions in graphene. Nature 438, 197 (2005)
24. Berger C, Song ZM et al. Ultrathin Epitaxial Graphite: 2D Electron Gas Properties and a Route toward Graphene-based Nanoelectronics. J. Phys. Chem. B 108, 19912 (2004)
25. Li XS, Cai WW, Ruoff RS et al. Large-Area Synthesis of High-Quality and Uniform Graphene Films on Copper Foils. Science 324, 1312 (2009)
26. Lin YC, Jin C, Lee JC, Jen SF, Suenaga K and Chiu PW. Clean Transfer of Graphene for Isolation and Suspension. ACS Nano 5, 2362 (2011)
27. Baraton L, Cojocaru CS and Pribat D. Process for controlled growth of graphene films. Patent EN 0805769-2008 (2008)
28. Lee CS, Baraton L, He Z, Maurice JL, Chaigneau M, Pribat D and Cojocaru CS. Dual graphene films growth process based on plasma-assisted chemical vapor deposition. SPIE proceedings 7761, 77610P (2010)
29. Lee CS, Maurice JL et al. Synthesis of conducting transparent graphite layers directly on functional substrate at 450°C. To be submitted.
30. Sackin DM, Jr JHG, Gabriel KJ, Patton ME. Embedded microdevices for infrastructure monitoring. 16th congress of Iabse, Lucerne (2000).
31. Kelly RG, Jones SH. Development of an embeddable microinstrument for corrosivity monitoring in concrete, Final contract report. School of Engineering and Applied Science; Univeristy of Virginia (1999).
32. Cain RP, Carkhuff BG, Grossman KR, Weiskopf F. Packaging for a Sensor Platform Embedded in Concrete. MRS proceedings, symposium N (2001).